XIII Congresso Ibérico de Acústica
55º Congreso Español de Acústica
TECNIACÚSTICA 2024
Faro, 11 a 13 setembro 2024

MODELING AND OPTIMIZATION OF A LIGHTWEIGHT METAMATERIAL PARTITION FOR IMPROVED SOUND TRANSMISSION LOSS

M. Ribera[1], B. Van Damme[2], A. Pereira[1], P. Amado Mendes[1], L. Godinho[1]

[1] ISISE, ARISE, Departamento de Engenharia Civil, Universidade de Coimbra
e-mail: mrtejeda@uc.pt, {apereira, pamendes, lgodinho}@dec.uc.pt
[2] EMPA, Laboratory for Acoustics/Noise Control
e-mail: bart.vandamme@empa.ch

Abstract
The improvement of airborne sound insulation of partition walls has traditionally relied on methods such as increasing mass or incorporating additional material layers. Locally resonant acoustic metamaterials have demonstrated the potential to improve acoustic performance without a significant mass increment. Nonetheless, their implementation in building acoustic applications remains limited. In this work, an optimization procedure will be performed to derive optimal properties of periodically attached spring-mass resonators, using a 1D Finite Element (FE) model of a unit cell. Two cost functions are studied, one which maximizes the sound transmission loss in the coincidence region of the gypsum board panels, and one which maximizes the weighted sound reduction index defined in ISO 717-1. Constraints of the optimization variables are set with manufacturability in mind, and computations are performed using parallel multicore processing. A very efficient optimization approach is thus attained, obtaining optimal resonator properties to maximize transmission loss while minimizing the added mass, for both oblique and diffuse incidence.

Keywords: Acoustic Metamaterials, FEM, Sound transmission loss, Optimization, Building acoustics

PACS nº. 43.55.Ti, 43.55.Rg

1 Introduction

The field of metamaterials has evolved in recent years, attracting the interest of academia and industry for solutions with properties beyond those found in traditional materials. In the field of sound insulation, the implementation of vibroacoustic metamaterials is currently being investigated [1–8], aiming to provide lightweight solutions with superior noise and vibration performance. These solutions can be applied in various domains, including automotive, naval, aerospace, and building acoustics applications [1, 2].

Different design approaches have been proposed, including the use of topological optimization frameworks. By optimizing either the host structure [3] or the structural core [2], important improvements in the sound transmission loss in the target frequency range have been found at normal and oblique incidence angles for single and double panel configurations. These methods typically rely on gradient-based optimization algorithms, such as the Method of Moving Asymptotes (MMA) [3], often requiring several iterations and reaching a local minimum [4].

Another approach, more widely studied numerically and experimentally, is the distribution of local resonant subsystems at a subwavelength scale [1], commonly referred to as Locally Resonant Metamaterials (LRM). By exploiting Fano-type interference, stop bands inhibiting wave propagation can be opened at specific frequency ranges. Such stop bands can be beneficial for vibration and noise insulation, particularly when the target is to attenuate vibrations within a limited frequency range. The ability to tailor these stop bands through the design of the LRM provides a versatile tool for a wide array of applications.

Various experimental realizations of these approaches have been proposed, such as using serpentine or cantilever resonators [10], double lever resonators [1], and membrane resonators [11], with particular focus on automotive and aerospace applications [1]. Recently, inverse methodologies have been explored to design locally resonant metamaterials based on Machine Learning (ML) techniques [4, 5]. As opposed to standard topology optimization, these data-driven approaches can drastically reduce the computational cost of traditional numerical methods, thus being a highly efficient tool for the design of LRM [4].

In the present work, a FE model of a single-layered elastic wall is developed and validated. This model is then elaborated with idealized spring-mass systems periodically attached, allowing the proposal of an optimization approach. Two formulations of the optimization problem are studied, one which maximizes the Weighted Sound Reduction Index (R_w) and one which maximizes the Sound Transmission Loss (STL) around the critical frequency of the panel. Moreover, a multi-objective optimization is proposed, allowing the parameters of the LRM to be obtained that maximize sound transmission loss while minimizing the added mass of the resonators. The effect of the resonators is observed in terms of the sound transmission loss for oblique and diffuse incidence, as well as the flexural stop band created by the resonators.

2 Modeling and Optimization

2.1 FE model of wall partition

The partition wall is modeled as an elastic isotropic plate of thickness h, density ρ, Young's modulus E, Poisson's ratio ν, and internal loss factor η, which is subject to plane wave excitation with incidence angle θ (Figure 1). A single unit cell (UC) is modeled by imposing periodic boundary conditions, assuming thus a plate of infinite lateral dimensions. The LRM is introduced as a spring-mass system representing a resonator of mass m_r, and complex stiffness $K_r = K_r(1 + i\eta_s)$, accounting for structural damping by the spring loss factor η_s.

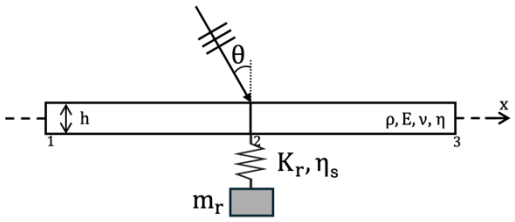

Figure 1 – Schematic drawing of the modeled unit cell.

The plate is built using Timoshenko beam elements to describe the flexural vibrations of the system [9]. To perform the model of the unit cell, a 1D Finite Element approach is chosen, thus requiring solving the equation of motion given by

$$(\mathrm{K} - \omega^2 \mathrm{M})\mathrm{u} = \mathrm{F}, \tag{1}$$

where u is the displacement vector, K and M are the stiffness and mass global matrices, F is the external force applied to the system and $\omega = 2\pi f$ the angular frequency. After obtaining the global matrix of the system, boundary conditions are imposed. Periodicity is imposed by applying Bloch-Floquet at the boundaries [12]

$$\mathrm{u}_1 = \mathrm{u}_2 \cdot \mathrm{e}^{-\mathrm{iqa}}, \qquad \mathrm{u}_3 = \mathrm{u}_2 \cdot \mathrm{e}^{\mathrm{iqa}}, \tag{2}$$

where q is the wavevector in the x direction and a the lattice constant.
The material properties of MDF and Gypsum boards used for the models are shown in Table 1.

Table 1 – Material properties.

Material	h [m]	ρ [kg/m^3]	E [GPa]	ν [-]	η [-]
MDF board	0.016	712	3.0	0.3	0.04
Gypsum board	0.0127	820	3.2	0.262	0.1

2.2 Sound Transmission Loss and Stopband prediction

The transmission coefficient $\tau(\omega, \theta)$ is obtained by computing the ratio between transmitted to incident pressure. Once the transmission coefficient τ is obtained, the oblique-incidence sound transmission loss, also referred to as sound reduction index, can be calculated [13]

$$\mathrm{STL_{obl}} = 10\log_{10}\frac{1}{\tau(\omega,\theta)}, \qquad \tau(\omega,\theta) = \left|\frac{p_{tr}}{p_{in}}\right|^2. \tag{3}$$

To estimate the random or diffuse incidence transmission loss, the angle-dependent transmission coefficient is integrated over all angles of incidence assuming equal sound intensity in all directions [12]

$$\mathrm{STL_{dif}} = -10\log_{10}\left(\frac{\int_{\theta=0}^{\theta_{\lim}} \tau(\omega,\theta)\cos(\theta)\sin(\theta)\,\mathrm{d}\theta}{\int_{\theta=0}^{\theta_{\lim}} \cos(\theta)\sin(\theta)\,\mathrm{d}\theta}\right), \tag{4}$$

where $\theta_{\lim}$ is the limiting angle of incidence. Considering a perfectly diffuse field, the limiting angle would be $\theta_{\lim} = 90^{\mathrm{o}}$. This does not occur in practice, and incident waves with close to normal incidence are more likely. To find a better fit with experimental results, the limiting angle can be truncated from 70º to 85º, finding a better agreement using $\theta_{\lim} \approx 78^{\mathrm{o}}$ for single panels [14].

As an alternative to evaluating the effect of the added resonators, their effect can be visualized in terms of the flexural vibration bandgaps by computing the band structure of the LRM panel. In this work, a direct methodology was implemented using a Transfer Matrix approach, efficiently obtaining the complex propagation constant of the UC considering Timoshenko beams with periodical resonators

[15]. If the resonators are tuned to the same frequency, the band gap limits for LRM-type structures can be estimated for 1D and 2D vibrating structures by [16]

$$\omega_r < \omega < \omega_r\sqrt{1 + M_r}\,, \tag{5}$$

where $\omega_r = \sqrt{K_r/m_r}$ is the resonant frequency of the resonator and $M_r = m_r/m_p$ is the resonator's mass ratio between the mass of the resonator and the mass of the panel.

2.3 Optimization

Next, two formulations are studied to maximize the acoustic performance of the metamaterial partition described in the previous section. The optimization variables correspond to the resonator's mass ratio, stiffness, and the loss factor.

$$\text{Maximize} \begin{cases} R_w & \text{(6a)} \\ \int_{f_l}^{f_u} STL_{meta}(\omega, M_r, K_r, \eta_s) - STL_{bare}(\omega)\, d\omega & \text{(6b)} \end{cases}$$

2.3.1 Optimization to Single-Value Rating

The first cost function consists of maximizing the Weighted Sound Reduction Index (R_w), a standardized single-number rating used to evaluate building elements' airborne sound insulation properties according to ISO 717-1 [17]. The full methodology will not be detailed in this paper for brevity. However, it is essential to point out that this rating considers reference values in one-third-octave bands from 100 Hz to 3150 Hz, thus frequencies outside of this range will not be considered during the evaluation of this optimization routine using the single-value rating.

Two scenarios of the optimization to R_w were tested, one in which the stiffness is set as optimization variable, and one in which the stiffness is set fixed, tuning the resonators to the critical frequency of the panel. This frequency is given by the lowest coincidence frequency occurring at grazing angle [12]

$$f_{co} = \frac{c_0^2}{2\pi \sin(\theta)}\sqrt{\frac{\rho h}{D}}, \tag{7}$$

where $D = Eh^3/[12(1-\nu^2)]$ is the bending stiffness of the wall and $c_0 = 343\ m/s$ the speed of sound in air. The critical frequency for the gypsum board panel is found to be around 2459 Hz.

2.3.2 Optimization to Sound Transmission Loss

The second cost function consists of maximizing the difference between the STL of the LRM panel and the bare panel, within a defined frequency range bounded by f_l and f_u. This formulation gives extra flexibility in finding optimized resonator parameters tuned to any given frequency range instead of the optimization using the single-number rating. The integral in equation (6) is calculated using trapezoidal numerical integration with a resolution of 1 Hz. Using this formulation required setting the stiffness as optimization variable, as the tuning will depend on the frequency limits set by f_l and f_u.

2.3.3 Implementation

Both modeling and optimization were performed in MATLAB. Three optimization solvers, MultiSearch, GlobalSearch, and a Genetic Algorithm were studied and compared, ensuring that a global solution is found. MultiSearch (MS) and GlobalSearch (GS) are gradient-based methods that allow to find local and global minimum of smooth problems, and mainly differ by how the starting points are generated, either through a fixed number of starting points or through a scatter-search mechanism [18], respectively.

On the other hand, the Genetic Algorithm (GA) is a stochastic, population-based method that uses evolutionary strategies such as selection, crossover, and mutation to search for the optimal solution [19]. Regardless of the solver used, constraints in the optimization variables are set identically, allowing the evaluation of a wide range of resonator configurations (Table 2), and the STL is evaluated both considering grazing and diffuse incidence through equations (3) and (4). In the case of equation (6b), f_l and f_u are set as optimization variables in a frequency range surrounding the critical frequency of the gypsum board.

Table 2 – Search space boundaries of the optimization variables.

Optimization variable	Symbol	Lower bound	Upper bound
Mass ratio	M_r	0.001	0.50
Stiffness	K_r	1.0e4	1.0e7
Loss Factor	η_s	0.01	0.10
Lower freq. bound	f_l	2100	2400
Upper freq. bound	f_u	2500	2800

Being GA populated-based, this approach is well suited for multi-objective optimization problems, which is explored in this work to find a resonator configuration that maximizes either R_w or STL and minimizes the Mass Ratio. The single-objective GA previously defined is modified to find a set of solutions on a single run, defining the Pareto Front. This was implemented using MATLAB's built-in *gamultiobj* function, which uses a variant of NSGA-II controlled elitist strategy [19].

Two approaches were explored for diffuse-incidence computations. The first consists of performing the optimization to the diffuse-field STL, evaluating equation (4) at each iteration. This configuration was tested on the optimization to R_w. The second approach simply takes the optimized parameters from the oblique incidence optimization. This configuration was tested on the optimization to STL. Calculations were performed using local parallel computing with a 10-core CPU on an Apple Silicon M1 Pro Chip.

3 Results

3.1 Model validation

Before inserting the resonators in the FE model, the model of the bare panel was validated experimentally (Figure 2a). The measurements were performed in the transmission chambers at the Swiss Federal Laboratories for Materials Science and Technology (EMPA) following standard EN ISO 10140 [20], considering a single MDF board of 1.23 by 1.48 m and a thickness of 16 mm. The material properties used for the models are shown in Table 1.

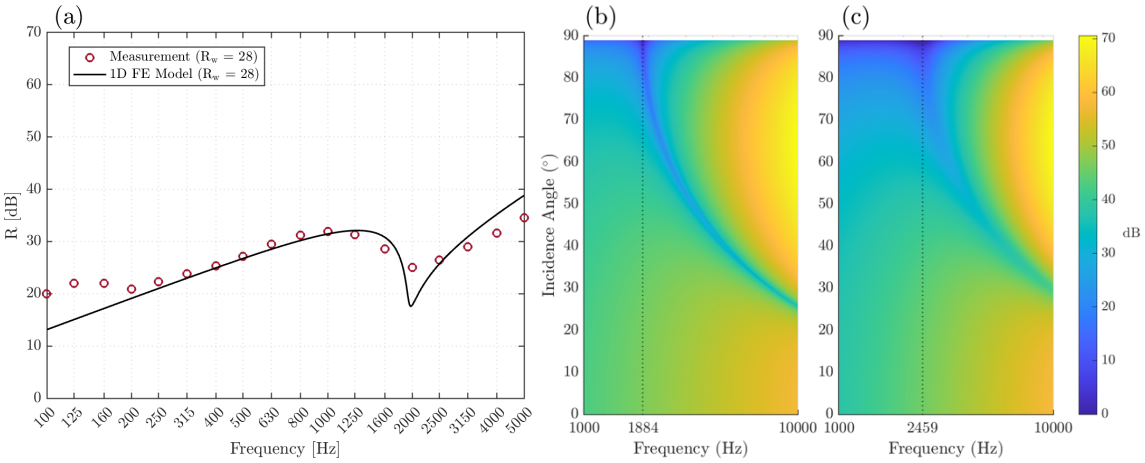

Figure 2 – (a) Measured and modeled sound transmission loss of single MDF board, and modeled Sound Transmission Loss as a function of frequency and angle of incidence of (b) MDF and (c) Gypsum boards.

Fair agreement can be found between both, finding analogous R_w values (Figure 2a). Differences between the modeled and the measurements of STL can be attributed to resonant transmission, given the small dimensions of the partition used for measurements and the assumption of a panel of infinite extent on the model. Best agreement was found by setting the limiting angle of incidence to 80°. Thus, further diffuse field calculations were performed identically.

The transmission loss can also be computed as a function of the incidence angle, shown here for MDF and gypsum board panels (Figure 2 b-c). This plot allows the visualization of the coincidence effect as a function of frequency and angle of incidence, which can be useful to visualize the effect of the added resonators. Following the validation, the resonators were inserted into the FE model of the gypsum board, using this model for the optimization.

3.2 Optimization to R_w

First, the optimization to the single value rating is evaluated at grazing incidence, where transmission is the highest and the coincidence effect at its lowest frequency, or critical. Both scenarios of enforced tunning and variable stiffness are compared in Figure 3.

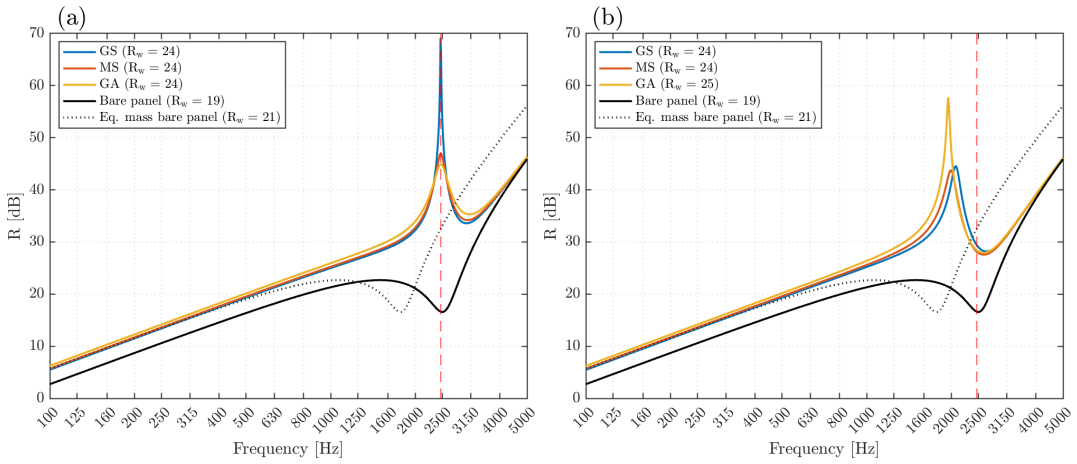

Figure 3 – Optimization to R_w at grazing incidence with (a) forced tuning resonators to critical frequency and (b) variable stiffness. The dashed vertical red line corresponds to the critical frequency.

When tuning the resonators to the critical frequency, a similar result is obtained from the three algorithms (Figure 3a). Compared to the bare panel, the coincidence dip is effectively suppressed by the resonators, while at higher frequencies, the curves converge. When comparing it to a panel of equivalent mass, it can be observed that the LRM panel still shows a higher R_w value while avoiding the shifted coincidence dip. Nonetheless, the equivalent mass panel provides higher insulation above the critical frequency.

When the stiffness is set as an optimization variable, the tuning of the resonators is not enforced, giving the algorithm the flexibility to modify the tuning. This might be detrimental, as results may vary considerably depending on the constraints chosen. As can be observed in Figure 3b, the tuning was found near the critical frequency, slightly shifted depending on the algorithm. This resulted in a dip at the critical frequency; however, in terms of the R_w, results are similar and even superior, in the case of the GA, finding a 1dB improvement.

3.3 Optimization to STL

The optimization is next performed with the integral cost function (equation (6b)), which maximizes the STL between f_l and f_u. The results of this optimization are shown in Figure 4.

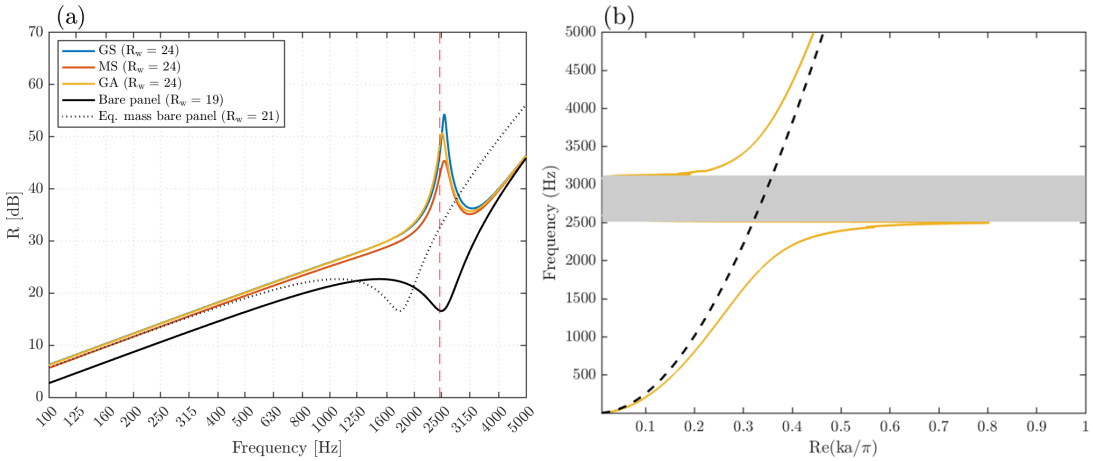

Figure 4 – (a) Optimization to STL at grazing incidence and (b) dispersion curves of LRM panel from GA. The dashed black line corresponds to the bare panel.

The three algorithms succeeded in tuning the resonators within the desired frequency range (Figure 4a). In all cases, the tuned frequency was slightly above the critical frequency. The dispersion curve shows the stopband created by the resonators in the bending wave with the optimized configuration obtained from the GA, which retrieved a mass ratio of $M_r = 0.49$ (Figure 4b). The upper limit is determined by this parameter (equation (5)), which is highly dependent on the upper bound set to this optimization variable since a higher added mass increases the overall STL.

Comparing the optimization to the single-value rating, a similar performance is obtained in terms of R_w, obtaining an improvement of 5dB from the three algorithms with the specified optimization variable boundaries (Table 2) compared to the bare panel. The optimization to STL, however, gives more flexibility to maximize the STL for any given frequency range, whether the limits are set fixed or set as optimization variables.

3.4 Diffuse-incidence optimization

Both optimization frameworks are now evaluated at diffuse incidence, and results are shown in Figure 5. The optimization considering all angles of incidence is assessed on the R_w optimization (solid line), while the simplified approach using the parameters from grazing incidence is evaluated with the STL optimization (dash-dotted line).

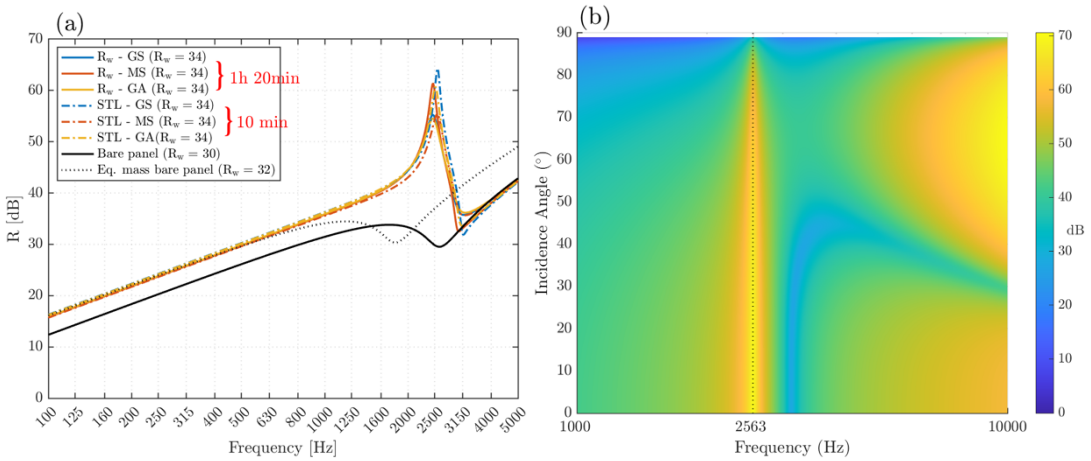

Figure 5 – (a) Optimization to R_w and STL at diffuse incidence, (b) STL of optimized metamaterial panel from STL – GS, as a function of frequency and angle of incidence.

Both approaches to obtaining the optimized diffuse incidence STL produced similar results in terms of sound insulation, even considering that each used a different cost function formulation. In terms of the single-value rating, identical R_w values were found. Compared to the oblique incidence results, there is a more pronounced dip following the resonator peak, which in some configurations, such as the STL – GS, can cross below the bare panel STL curve. This effect is visualized for the optimization results of this configuration (Figure 5b). This new dip can be identified as the bending of the coincidence dip, becoming critical at normal incidence. Although detrimental, particularly at normal incidence, this dip remains above the bare panel STL curve for most configurations.

These results suggest that using the optimized parameters at grazing incidence optimization gives a good approximation, eliminating the need to perform the optimization for all angles of incidence. This is beneficial since the optimization to diffuse incidence becomes notably more computationally expensive than optimizing to a single angle, even with a powerful CPU and multiple processes parallelized.

3.5 Multi-objective optimization

So far, optimizing using single-objective has resulted in resonator designs with mass ratios close to or at the upper bound of this optimization variable, as a higher added mass translates into higher sound insulation. To find an optimized resonator configuration that minimizes the added mass, the multi-objective is performed using a GA for the R_w and STL optimization at grazing incidence and then calculated at diffuse incidence using the retrieved optimized parameters. The solutions were filtered, removing those where the added mass was too low to get any improvement in STL. The filtered results for the optimization to R_w and STL are shown in Figure 6, plotting the maximum and minimum mass ratio value cases and an intermediate case.

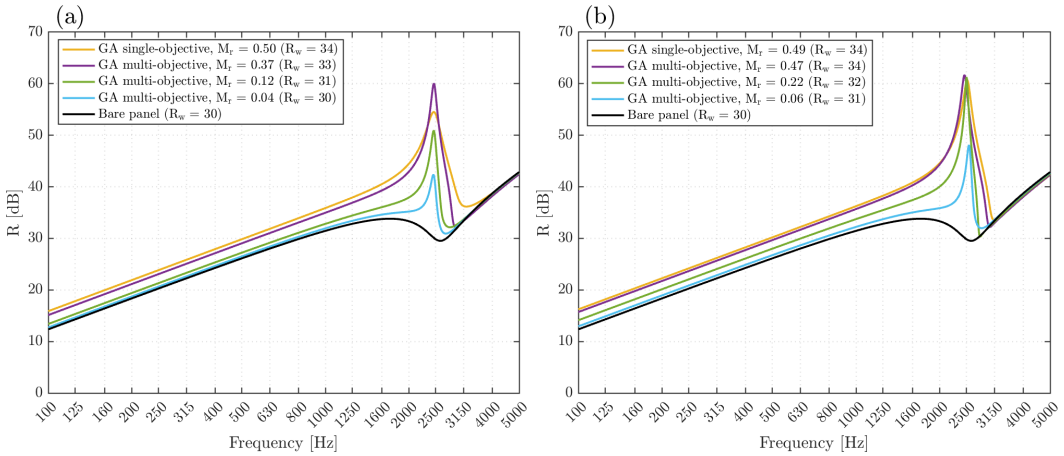

Figure 6 – Filtered multi-objective optimization at diffuse incidence to (a) R_w and (b) STL.

No single global solution is found by the algorithm. Instead, a set of solutions that balance any of the two objectives is found. Compared to the previous single-objective results (Figure 5a), a significant decrease in M_r is obtained, finding LRM configurations with a mass ratio as small as 4%. Although a more modest R_w improvement is obtained, the coincidence dip is suppressed while the added mass is kept at a minimum. As the added mass decreases, the peak becomes narrower along the upper limit of the bandgap. One way to address the narrow improvement from this configuration can be by considering multimodal resonator configurations. Nonetheless, it must be ensured that such solution maintains an equivalent or inferior added mass compared to the single-resonator configuration.

4 Conclusions

In the present study, an efficient FE model was developed and validated. This simplified model employs idealized spring-mass resonators, enabling an effective optimization framework to achieve multiple metamaterial configurations that maximize sound transmission loss while minimizing the added mass from the resonators. Two optimization formulations are studied, which enable the maximization of either the R_w or the STL within a limited frequency range. Both formulations produced comparable results under oblique and diffuse incidence. It is shown that the complete optimization for all angles of incidence yields equivalent results to using the results from the optimization at grazing incidence for diffuse calculation, thus significantly reducing computation times. This optimization framework offers flexibility in designing metamaterials, enabling the evaluation of various LRM designs. Future work includes modeling and optimizing multimodal LRM panels using inverse techniques, extending this model to multiple-panel partitions, and the experimental study and validation of these optimized metamaterial partition designs.

Acknowledgments

This work was partly financed by FCT / MCTES through national funds (PIDDAC) under the R&D Unit Institute for Sustainability and Innovation in Structural Engineering (ISISE), under reference UIDB / 04029/2020, and under the Associate Laboratory Advanced Production and Intelligent Systems ARISE, under reference LA/P/0112/2020. This work was developed in the scope of the Marie Sklodowska-Curie Actions through the Horizon Europe DN METAVISION project (GA 101072415).

References

[1] F. A. Pires, *Design Strategies for Narrow and Broadband Noise and Vibration Reduction through Distributed Resonators*. PhD thesis, KU Leuven, Faculty of Engineering Science, 2023.

[2] V. Cool, O. Sigmund, N. Aage, F. Naets, and E. Deckers, "Vibroacoustic topology optimization for sound transmission minimization through sandwich structures," *Journal of Sound and Vibration*, vol. 568, p. 117959, 2024.

[3] D. Giannini, M. Schevenels, and E. P. Reynders, "Optimization of material thickness distribution in single and double partition panels for maximized sound insulation," *Structural and Multidisciplinary Optimization*, vol. 66, no. 12, p. 243, 2023.

[4] S. Dedoncker, C. Donner, L. Taenzer, and B. Van Damme, "Generative inverse design of multimodal resonant structures for locally resonant metamaterials," *arXiv preprint arXiv:2309.04177*, 2023.

[5] C. Song, X. Wang, S. Xu, C. Zhao, and Z. Huang, "Inverse design of laminated plate-type acoustic metamaterials for sound insulation based on deep learning," *Applied Acoustics*, vol. 218, p. 109906, 2024.

[6] A. J. Hall, V. Sorokin, M. Aghamohammadi, G. Dodd, G. Schmid, Y. Yang, and B. Mace, "Sound transmission loss of periodic mindlin plates with non-uniformly spaced mass attachments," *The Journal of the Acoustical Society of America*, vol. 155, no. 3, pp. 2199–2208, 2024.

[7] Y. Zou, Z. Wang, P. Adjei, and X. Zhao, "The sound insulation performance of light wood frame construction floor structure based on phononic crystal theory," *Journal of Building Engineering*, vol. 75, p. 107039, 2023.

[8] D. Giannini, M. Schevenels, and E. P. Reynders, "Rotational and multimodal local resonators for broadband sound insulation of orthotropic metamaterial plates," *Journal of Sound and Vibration*, vol. 547, p. 117453, 2023.

[9] P. Amado-Mendes, L. Godinho, M. Jovanoska, P. Amaral, and N. Pinho, "Effect of embedded resonators in sound insulation panels-a numerical study," in *INTER-NOISE and NOISE-CON Congress and Conference Proceedings*, vol. 259, pp. 8131–8140, Institute of Noise Control Engineering, 2019.

[10] J. H. Vazquez Torre, J. Brunskog, V. Cutanda Henriquez, and J. Jung, "Hybrid analytical-numerical optimization design methodology of acoustic metamaterials for sound insulation," *The Journal of the Acoustical Society of America*, vol. 149, no. 6, pp. 4398–4409, 2021.

[11] X. Wang, X. Luo, H. Zhao, and Z. Huang, "Acoustic perfect absorption and broadband insulation achieved by double-zero metamaterials," *Applied Physics Letters*, vol. 112, no. 2, 2018.

[12] N. Jimenez, O. Umnova, and J.-P. Groby, "Acoustic waves in periodic structures, metamaterials, and porous media," *Ch. the Transfer Matrix Method in Acoustics, Springer International Publishing, Cham*, pp. 103–164, 2021.

[13] J. H. Rindel, *Sound insulation in buildings*. CRC Press, 2017.

[14] H.-J. Kang, J.-G. Ih, J.-S. Kim, and H.-S. Kim, "Prediction of sound transmission loss through multilayered panels by using gaussian distribution of directional incident energy," *The Journal of the Acoustical Society of America*, vol. 107, no. 3, pp. 1413–1420, 2000.

[15] D. Yu, Y. Liu, G. Wang, H. Zhao, and J. Qiu, "Flexural vibration band gaps in timoshenko beams with locally resonant structures," *Journal of applied physics*, vol. 100, no. 12, 2006.

[16] C. Sugino, Y. Xia, S. Leadenham, M. Ruzzene, and A. Erturk, "A general theory for bandgap estimation in locally resonant metastructures," *Journal of Sound and Vibration*, vol. 406, pp. 104–123, 2017.

[17] International Organization for Standardization, "Acoustics — Rating of sound insulation in buildings and of building elements — Part 1: Airborne sound insulation," 2013. ISO 717-1:2013.

[18] M. Ribera, "Acoustic characterization of porous materials using a PU probe", Master's thesis, Erasmus Mundus Master WAVES, 2023.

[19] A. Konak, D. W. Coit, and A. E. Smith, "Multi-objective optimization using genetic algorithms: A tutorial," *Reliability engineering & system safety*, vol. 91, no. 9, pp. 992–1007, 2006.

[20] International Organization for Standardization, "Acoustics — Laboratory measurement of sound insulation of building elements — Part 2: Measurement of airborne sound insulation," 2021. ISO 10140-2:2021.